

**REPORT DOCUMENTATION PAGE**

Form Approved  
OMB No. 0704-0188

The public reporting burden for this collection of information is estimated to average 1 hour per response, including the time for reviewing instructions, searching existing data sources, gathering and maintaining the data needed, and completing and reviewing the collection of information. Send comments regarding this burden estimate or any other aspect of this collection of information, including suggestions for reducing the burden, to the Department of Defense, Executive Services and Communications Directorate (0704-0188). Respondents should be aware that notwithstanding any other provision of law, no person shall be subject to any penalty for failing to comply with a collection of information if it does not display a currently valid OMB control number.

**PLEASE DO NOT RETURN YOUR FORM TO THE ABOVE ORGANIZATION.**

1. REPORT DATE (DD-MM-YYYY) 14-02-2012		2. REPORT TYPE Conference Proceedings		3. DATES COVERED (From - To)	
4. TITLE AND SUBTITLE Some Insights of Spectral Optimization in Ocean Color Inversion				5a. CONTRACT NUMBER	
				5b. GRANT NUMBER	
				5c. PROGRAM ELEMENT NUMBER 0602435N	
6. AUTHOR(S) ZhongPing Lee, B. Franz, S. Shang, Q. Dong, Robert Amone				5d. PROJECT NUMBER	
				5e. TASK NUMBER	
				5f. WORK UNIT NUMBER 73-6287-A1-5	
7. PERFORMING ORGANIZATION NAME(S) AND ADDRESS(ES) Naval Research Laboratory Oceanography Division Stennis Space Center, MS 39529-5004				8. PERFORMING ORGANIZATION REPORT NUMBER NRL/PP/7330-11-0813	
9. SPONSORING/MONITORING AGENCY NAME(S) AND ADDRESS(ES) Office of Naval Research One Liberty Center 875 North Randolph Street, Suite 1425 Arlington, VA 22203-1995				10. SPONSOR/MONITOR'S ACRONYM(S) ONR	
				11. SPONSOR/MONITOR'S REPORT NUMBER(S)	
12. DISTRIBUTION/AVAILABILITY STATEMENT Approved for public release, distribution is unlimited.					
20120217346					
13. SUPPLEMENTARY NOTES					
14. ABSTRACT Over the past few decades, various algorithms have been developed for the retrieval of water constituents from the measurement of ocean color radiometry, and one of those approaches is spectral optimization. This approach defines an error function (or cost function) between the observed spectral remote sensing reflectance and an estimated spectral remote sensing reflectance over the range of observed wavelengths, with the latter modeled using a few variables that represent the optically active properties (such as the absorption coefficient of phytoplankton and the backscattering coefficient of particles). The values of the variables when the error function reaches a minimum are the optimized properties. The applications of this approach implicitly assume that there is only one global minimum condition, and that any local minimum (if exist) can be avoided through the numerical optimization scheme. Here, with data from numerical simulations, we show the shape of the error surface as a mechanism to visualize the solution space for the model variables. Further, using two established models as examples, we demonstrate how the solution space changes under different model assumptions as well as the impacts on the quality of the retrieved water properties.					
15. SUBJECT TERMS ocean color remote sensing, optimization, algorithm					
16. SECURITY CLASSIFICATION OF:			17. LIMITATION OF ABSTRACT UU	18. NUMBER OF PAGES 11	19a. NAME OF RESPONSIBLE PERSON Robert Amone
a. REPORT Unclassified	b. ABSTRACT Unclassified	c. THIS PAGE Unclassified			19b. TELEPHONE NUMBER (Include area code) 228-688-5268

# Some insights of spectral optimization in ocean color inversion

Zhongping Lee<sup>a</sup>, Bryan Franz<sup>b</sup>, Shaoling Shang<sup>c</sup>, Qiang Dong<sup>d</sup>, Robert Arnone<sup>e</sup>

<sup>a</sup> Environmental Earth and Ocean Sciences, University of Massachusetts at Boston, 100 Morrissey Blvd, Boston, MA 02125; Zhongping.Lee@umb.edu

<sup>b</sup> NASA Goddard Space Flight Center, Greenbelt, MD, 20771

<sup>c</sup> State Key Laboratory of Marine Environmental Science, Xiamen University, 361005, China

<sup>d</sup> Geosystems Research Institute, Mississippi State University, Stennis Space Center, MS 39529

<sup>e</sup> Naval Research Laboratory, Stennis Space Center, MS 39529

## ABSTRACT

Over the past few decades, various algorithms have been developed for the retrieval of water constituents from the measurement of ocean color radiometry, and one of those approaches is spectral optimization. This approach defines an error function (or cost function) between the observed spectral remote sensing reflectance and an estimated spectral remote sensing reflectance over the range of observed wavelengths, with the latter modeled using a few variables that represent the optically active properties (such as the absorption coefficient of phytoplankton and the backscattering coefficient of particles). The values of the variables when the error function reaches a minimum are the optimized properties. The applications of this approach implicitly assume that there is only one global minimum condition, and that any local minimum (if exist) can be avoided through the numerical optimization scheme. Here, with data from numerical simulations, we show the shape of the error surface as a mechanism to visualize the solution space for the model variables. Further, using two established models as examples, we demonstrate how the solution space changes under different model assumptions as well as the impacts on the quality of the retrieved water properties.

**Keywords:** ocean color remote sensing, optimization, algorithm

## 1. INTRODUCTION

The spectral distribution of reflected Sun light upwelling from beneath the ocean surface, which is often referred to as remote-sensing reflectance or  $R_{rs}(\lambda)$ , contains information on the composition of in-water constituents and forms the basis to retrieve such information from satellite measured radiance. Historically, the methods to quantitatively retrieve such information from ocean color radiometry include simple empirical regression techniques [1, 2], algebraic solutions [3, 4], and spectral optimization [5-7] of modeled spectrum based on inherent optical properties (IOP). One such spectral optimization algorithm (SOA) was proposed in the Coastal Zone Color Scanner (CZCS) era [8]. However, because it searches for the optimal set of solutions among numerous candidates for each measured reflectance spectrum, SOA was associated with large computational burden that consequently limited its application in processing satellite-measured ocean color images. In the recent decade, due to the rapid advancement of computer hardware and software, computation burden has become less critical and there is renewed interest in using SOA as an operational tool to process satellite ocean color data [9-11] from modern sensors such as Sea-viewing Wide Field-of-view Sensor (SeaWiFS), Moderate Resolution Imaging Spectroradiometer (MODIS), and Medium Resolution Imaging Spectrometer (MERIS).

Various SOA schemes have been developed in the past three decades (e.g., [6, 7, 12, 13]). Two such algorithms include the Hyperspectral Optimization Process Exemplar (HOPE) model [5, 14] and the Garver-Siegel-Maritorena (GSM) model [15]. As with other published approaches, HOPE and GSM assume a spectral shape (or eigenvector) for the component IOPs (i.e., absorption due to phytoplankton and yellow substance, backscattering due to particles) and retrieve the optimal magnitudes (or eigenvalue) of those eigenvectors that best reproduce the spectral distribution of the observed ocean color signal. The principal differences between the models, therefore, rest with the assumed spectral

shapes of the component IOPs. The optimization schemes applied to these models assume that there is no local minimum in the error function or that any such local minimum can be overcome by an optimization scheme (e.g., [16-18]). Here, using data from numerical simulations, we visualize the shape of the solution space and demonstrate that the error function has a clearly defined global minimum. More importantly, we show that the assumed spectral models have significant consequences on the closure between measured and modeled remote sensing reflectance and thus on retrievals of spectral optical properties.

## 2. BRIEF REVIEW OF SOA

For optically deep waters, the spectral reflectance upwelling from beneath the ocean surface,  $R_{rs}$ , can be modeled as a function of total absorption and total backscattering coefficients of the water column [19, 20], i.e.,

$$R_{rs}(\lambda) = Fun(a(\lambda), B(\lambda)) \quad (1)$$

where  $a(\lambda)$  and  $B(\lambda)$  are the spectral absorption and backscattering coefficients, respectively.

For SOA, an error function is defined and minimized to derive the optimal model variables, i.e.,

$$\delta_{R_{rs}} = \frac{\sqrt{\int_{\lambda_1}^{\lambda_2} (\tilde{R}_{rs}(\lambda) - R_{rs}(\lambda))^2}}{\int_{\lambda_1}^{\lambda_2} R_{rs}(\lambda)} = \sqrt{n} \frac{\sqrt{\sum_{\lambda_1}^{\lambda_2} (\tilde{R}_{rs}(\lambda) - R_{rs}(\lambda))^2}}{\sum_{\lambda_1}^{\lambda_2} R_{rs}(\lambda)} \quad (2)$$

where  $\int_{\lambda_1}^{\lambda_2}$  represents the average of a spectrum between wavelengths of  $\lambda_1$  and  $\lambda_2$  ( $n$  is the number of spectral bands),  $R_{rs}(\lambda)$  is the spectrum from measurements, while  $\tilde{R}_{rs}(\lambda)$  is the spectrum from modeling.

Typically,  $a(\lambda)$  and  $B(\lambda)$  are modeled as spectral functions of a series of scalar variables  $X_i$ , with  $i$  generally equal to or greater than 3.  $\tilde{R}_{rs}(\lambda)$  then becomes a function of  $X_i$ , and  $\delta_{R_{rs}}$  in general is:

$$\delta_{R_{rs}} = Fun(X_i) \quad (3)$$

In spectral optimization, for a given  $R_{rs}(\lambda)$ , the values of  $X_i$  are optimal when  $\delta_{R_{rs}}$  reaches a minimum. For all SOA schemes, although there are subtle differences in handling the IOP to AOP model (Eq. 1) and the error function (Eq. 2), most of the differences are embedded in the spectral models of  $a(\lambda)$  and  $B(\lambda)$ . For example, when the spectrum of particle backscattering is modeled as a power-law function of wavelength [1], the exponent value is 1.03 in the GSM [15], while it varies with  $R_{rs}(\lambda)$  in HOPE [3]. Further, because of the different spectral models, different SOAs may have different  $\delta_{R_{rs}}^{min}$  (minimized  $\delta_{R_{rs}}$ ) (Figure 1a) or identical  $\delta_{R_{rs}}^{min}$  but  $\tilde{R}_{rs}(\lambda)$  matches  $R_{rs}(\lambda)$  at different wavelengths (Figure 1b). Because of such characterizations, SOA schemes are not the same, and the assumed spectral treatment of the  $a(\lambda)$  and  $B(\lambda)$  in individual SOA schemes is the primary driver for differences in remote-sensing retrievals (see examples in IOCCG Report #5 [21]).

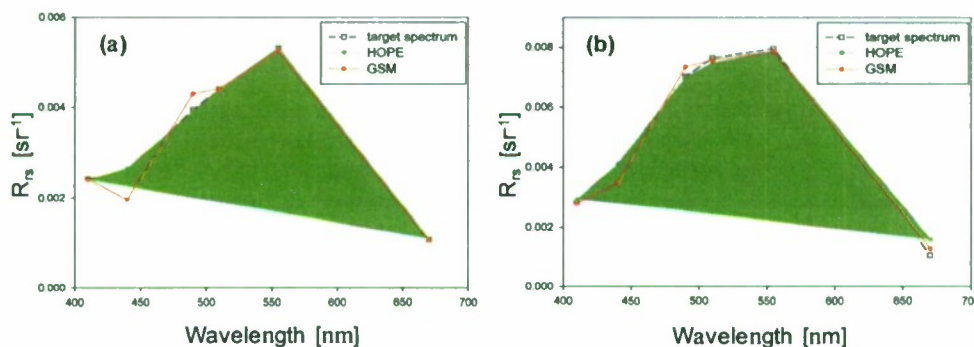


Figure 1. Examples of target and optimized spectral remote sensing reflectance. (a) HOPE and GSM achieved different degree of goodness of fit; (b) HOPE and GSM achieved identical goodness of fit, but the matching is different spectrally.

Compared with algebraic solutions, where all derivation steps are explicit, the solution steps of an SOA (i.e., numerical trial-and-error) are in general not explicit. To be able to have an unequivocal solution with an SOA scheme,  $\delta_{R_{rs}}$  must have a global minimum, and the design of the computer software must be able to overcome local minima if they exist. It is therefore useful to know the surface shape of  $\delta_{R_{rs}}$ , especially around the value of  $\delta_{R_{rs}}^{min}$ . For instance, if the surface

shape of  $\delta_{R_{rs}}$  resembles the letter U, i.e., it changes very slowly around  $\delta_{R_{rs}}^{min}$  for changing  $X_i$ , it will result in either more computation time to reach  $\delta_{R_{rs}}^{min}$  and/or ambiguity (large uncertainties) in the derived  $X_i$  values. On the other hand, if the surface shape of  $\delta_{R_{rs}}$  resembles the letter V, i.e., it changes sharply around  $\delta_{R_{rs}}^{min}$  for changing  $X_i$ , it will result in less computation time to reach  $\delta_{R_{rs}}^{min}$  and less or no ambiguity in the derived  $X_i$  values.

### 3. DATA AND METHODS

#### 3.1 Model of $R_{rs}$

Many studies were carried out in the past decades to find a suitable and accurate function to represent Eq. 1 (see review in Lee et al [22]). Without loss of generality, and to be consistent with an earlier effort (GSM), here the model of Gordon et al [19] is used to calculate sub-surface remote-sensing reflectance ( $r_{rs}$ ) from absorption and backscattering coefficients:

$$r_{rs} = \left(0.0949 + 0.0794 \frac{B}{a+B}\right) \frac{B}{a+B} \quad (4)$$

This  $r_{rs}$  is propagated through the surface to get the above-surface remote sensing reflectance ( $R_{rs}$ )

$$R_{rs} = \frac{0.52 r_{rs}}{1 - 1.7 r_{rs}} \quad (5)$$

#### 3.2 Data

The simulated dataset by the IOCCG Algorithm Working Group [21] is used in this study, which contains 500 spectral  $R_{rs}$  and the corresponding spectral IOP components, with wavelengths spanning the range of 400 – 800 nm at 10 nm spectral resolution. The dataset was sub-sampled to obtain wavelengths at 410, 440, 490, 510, 555, and 670 nm, spectral bands that closely match the settings of SeaWiFS. The values at 555 nm are simple averages of values at 550 nm and 560 nm. For each spectrally sub-sampled data point,  $\tilde{R}_{rs}(\lambda)$  was calculated with  $a(\lambda)$  and  $B(\lambda)$  that were used as inputs for the Hydrolight simulations, and then  $\delta_{R_{rs}}$  is calculated. Figure 2 shows the distributions of  $\delta_{R_{rs}}$  of the 500 points when sub-sampled to SeaWiFS bands. The median value of  $\delta_{R_{rs}}$  for this closure test is ~6%, which is consistent with the conclusion of Gordon et al [19] as the particle phase functions used in the IOCCG simulation and that in Gordon et al [19] are not identical. Note that in the inversion process (no matter which scheme), it is always considered that Eq. 4 is error free, so this model introduced difference will be propagated to the derived properties.

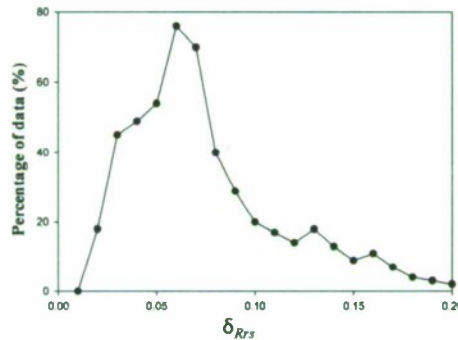


Figure 2. Distribution of “error” of Gordon et al [19]  $R_{rs}$  model.

#### 3.3 Spectral model of IOPs

$\delta_{R_{rs}}$  is a complex function of  $X_i$  used to generate spectral  $R_{rs}$ . Defining the number of variables as N and the number of spectral bands of  $R_{rs}$  as n (n has to be equal to or greater than N for possible solutions),  $\delta_{R_{rs}}$  may reach 0 when n=N and increases with the value of (n-N) if  $R_{rs}$  is not spectrally correlated. For easier demonstrations and following a widely

applied practice, we selected a three-parameter model system [23] to calculate  $\tilde{R}_{rs}(\lambda)$ . Basically, spectral  $a(\lambda)$  and  $B(\lambda)$  are modeled as

$$a(\lambda) = a_w(\lambda) + a_{ph}(\lambda) + a_{dg}(\lambda) \quad (6)$$

$$B(\lambda) = B_w(\lambda) + B_p(\lambda) \quad (7)$$

$a_w(\lambda)$  and  $B_w(\lambda)$  are values of water molecules and are considered universal constants (although they may change slightly with temperature and salinity [24]), with  $a_{ph}(\lambda)$ ,  $a_{dg}(\lambda)$  and  $B_p(\lambda)$  the absorption spectra of phytoplankton and detritus-gelbstoff and backscattering spectrum of suspended particles, respectively. Thus there are three unknown spectra ( $a_{ph}(\lambda)$ ,  $a_{dg}(\lambda)$  and  $B_p(\lambda)$ ) in Eq. 5, and they are further modeled as

$$a_{ph}(\lambda) = X_1 \tilde{a}_{ph}(\lambda) \quad (8)$$

$$a_{dg}(\lambda) = X_2 \tilde{a}_{dg}(\lambda) \quad (9)$$

$$B_p(\lambda) = X_3 \tilde{B}_p(\lambda) \quad (10)$$

$X_{1-3}$  are the three scalar variables to be derived from a measured  $R_{rs}$  via SOA.  $\tilde{a}_{ph}(\lambda)$ ,  $\tilde{a}_{dg}(\lambda)$  and  $\tilde{B}_p(\lambda)$  are spectral models (eigenvectors) determined based on field measurements [6, 7, 25, 26] or optimized from field-measured remote-sensing reflectance and concentration of chlorophyll [15].

In general,  $\tilde{a}_{dg}(\lambda)$  and  $\tilde{B}_p(\lambda)$  can be described as [1, 27]:

$$\tilde{a}_{dg}(\lambda) = e^{-S(\lambda-\lambda_0)} \quad (11)$$

$$\tilde{B}_p(\lambda) = \left(\frac{\lambda_0}{\lambda}\right)^Y \quad (12)$$

The spectral slope ( $S$ ) of  $\tilde{a}_{dg}(\lambda)$  and the power coefficient ( $Y$ ) are not constants for global waters. To reduce variables,  $S$  is set as  $0.015 \text{ nm}^{-1}$  in HOPE, but  $0.0206 \text{ nm}^{-1}$  in GSM; while  $Y$  changes with  $R_{rs}$  in HOPE, but is fixed as 1.03 in GSM. The reference wavelength ( $\lambda_0$ ) is generally set as 440 nm.

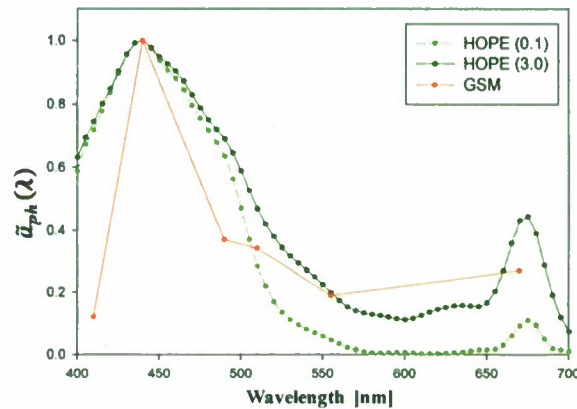


Figure 3. Comparison of the  $a_{ph}$  spectral shapes used in HOPE and GSM. #'s in the parenthesis indicate likely concentration of chlorophyll.

It is much more difficult to precisely model spectral  $\tilde{a}_{ph}(\lambda)$  [13, 26, 28, 29], although better fits could be achieved by increasing the number of free variables. As an example, we selected two simple models (where  $a_{ph}(\lambda)$  is modeled with one variable) to evaluate their impacts: one is the  $\tilde{a}_{ph}(\lambda)$  in HOPE, for which the spectral shape varies with the value of  $a_{ph}(440)$  (which is equivalent to chlorophyll concentration); and one is the  $\tilde{a}_{ph}(\lambda)$  in GSM, which is constant for

global waters. Figure 3 shows examples of the  $\tilde{a}_{ph}(\lambda)$  for various eutrophication states, and the following provides a mathematical expression of the two approaches:

HOPE:

$$\tilde{a}_{ph}(\lambda) = a_0(\lambda) + a_1(\lambda) \ln(a_{ph}(440)) \quad (13)$$

GSM:

$$\tilde{a}_{ph}(\lambda) = A_{ph-GSM}(\lambda) \quad (14)$$

Using SeaWiFS band setup as an example, there are  $R_{rs}$  data at 6 bands (411, 443, 490, 510, 555, and 670 nm) that are generally useful for remote sensing retrieval of in-water constituents. Data at the longer wavelengths are used for atmospheric corrections.

### 3.4 Optimization setups and software

For all numerical solutions, a set of initial values (first guess) is required to start the process. In HOPE, the initial values of the three variables are not kept constant, but are estimated for each given  $R_{rs}(\lambda)$  as follow:

$$X_1 = 0.05 \left( \frac{R_{rs}(440)}{R_{rs}(555)} \right)^{-1.5} \quad (15)$$

$$X_2 = X_1 \quad (16)$$

$$X_3 = 20 (0.06 + 0.3 X_1) R_{rs}(555) \quad (17)$$

Note that  $X_1$  represents  $a_{ph}(440)$  in HOPE. For GSM, the same starting values are used, but in this case  $X_1$  represents Chl, so  $a_{ph}(440)$  is converted to Chl following Eq. 8 by dividing the corresponding chlorophyll-specific value ( $a^*_{ph}(440)$ ) at 440 nm.

To generate physically meaningful solutions, boundaries of the three variables have to be set up, and they are (for HOPE):

$$0.002 \leq X_1 \leq 1.0 \text{ m}^{-1};$$

$$0.002 \leq X_2 \leq 5.0 \text{ m}^{-1};$$

$$0.0001 \leq X_3 \leq 0.5 \text{ m}^{-1}.$$

When using the  $a_{ph}(\lambda)$  model of GSM, while the boundaries for  $X_2$  and  $X_3$  are kept the same,  $X_1$  (for Chl) is set as

$$0.02 \leq X_1 \leq 100 \text{ mg m}^{-3}.$$

To derive the 3 scalar variables for each  $R_{rs}(\lambda)$ , we used the Solver tool included in Microsoft Excel. This tool uses several algorithms to find optimal solutions that include the Generalized Reduced Gradient Nonlinear Solving Method developed by Lasdon et al [30] and the Simplex LP Solving Method implemented by Fylstra et al [31].

After the optimization is reached for each  $R_{rs}(\lambda)$ , we not only recorded the  $\delta_{Rrs}^{min}$  (the global minimum of  $\delta_{Rrs}$ ), but also the difference between the derived spectral IOPs and the known spectral IOPs, which is calculated using Eq. 2, except that  $\tilde{R}_{rs}(\lambda)$  is replaced by the spectral IOPs that formed the optimized  $\tilde{R}_{rs}(\lambda)$ , and  $R_{rs}(\lambda)$  is replaced by the corresponding known spectral IOPs. We calculated  $\delta_a$  (for total absorption coefficient),  $\delta_{Bp}$  (for particle backscattering coefficient),  $\delta_{aph}$  (for phytoplankton absorption coefficient), and  $\delta_{adg}$  (for CDOM/gelbstoff coefficient), respectively. The wavelength range for these IOPs are from 410 nm to 555 nm, as there is limited information that can be derived in the longer wavelengths for most oceanic waters. These  $\delta_{IOP}$  values provide a measure of the goodness of the derived spectral inherent optical properties.

## 4. RESULTS AND DISCUSSIONS

The surface shape of  $\delta_{Rrs}$  provides an indicator of the effectiveness of an SOA approach. For the spectral IOP models evaluated here, examples of the surface shapes are presented in Figure 4, while the overall distributions of  $\delta_{Rrs}^{min}$  are shown in Figure 5.

#### 4.1 $\delta_{Rrs}$ surface

Figure 4 shows examples of  $\delta_{Rrs}$  (expressed as the percentage change of  $\delta_{Rrs}$  in relation to the percentage of change of  $a_{ph}$ ,  $a_{dg}$ , and  $B_p$ ) of both HOPE and GSM models. Generally,  $\delta_{Rrs}$  is monotonic in relation to  $X_i$  before and after  $\delta_{Rrs}$  reaches its global minimum. To understand the shape of  $\delta_{Rrs}$ , consider a simplified  $R_{rs}$  model where the total backscattering and total absorption spectra are modeled as one variable, respectively, then the model of remote sensing reflectance can be simplified as

$$\tilde{R}_{rs}(\lambda) = A(\lambda) \frac{B'_w(\lambda) + B_{nw}}{a'_w(\lambda) + a_{nw}} \quad (18)$$

Here,  $B'_w(\lambda)$  and  $a'_w(\lambda)$  are spectra associated with the backscattering and absorption coefficients of pure seawater, respectively, and are considered as constant; and  $B_{nw}$  and  $a_{nw}$  are two scalar variables for the backscattering and absorption coefficients of non-water constituents, respectively.  $A(\lambda)$  represents a combination of the spectral shapes of the two components and is constant for a given  $R_{rs}(\lambda)$ .

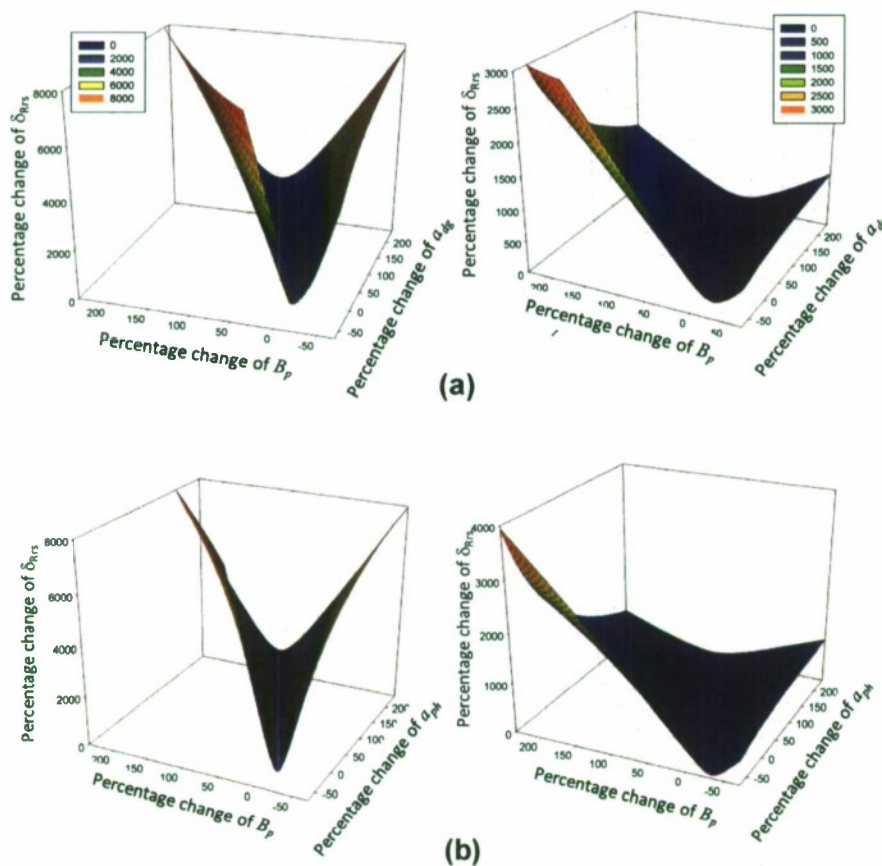


Figure 4. (a) Examples of surface shape of  $\delta_{Rrs}$  resulted from change of  $B_p$  and  $a_{dg}$ . (left) HOPE; (right) GSM; (b) Examples of surface shape of  $\delta_{Rrs}$  resulted from change of  $B_p$  and  $a_{ph}$ . (left) HOPE; (right) GSM.

With such a simplified model, we examine the variation of  $R_{rs}$  resulting from the change of  $B_{nw}$  and  $a_{nw}$ . Note that, since the denominator of Eq. 2 is a fixed value for a given  $R_{rs}(\lambda)$  (does not change with  $X_i$ ), the SOA is optimal when the following error-measure reaches a minimum,

$$\Delta_{Rrs} = \sum_{\lambda_1}^{\lambda_2} \left( \tilde{R}_{rs}(\lambda) - R_{rs}(\lambda) \right)^2 \quad (19)$$

And,  $\Delta_{Rrs}$  changes with  $B_{nw}$  through

$$\frac{\partial \Delta_{Rrs}}{\partial B_{nw}} = 2 \sum_{\lambda_1}^{\lambda_2} \left( A(\lambda) \frac{B_w(\lambda) + B_{nw}}{a_w(\lambda) + a_{nw}} - R_{rs}(\lambda) \right) \frac{A(\lambda)}{a_w(\lambda) + a_{nw}} \quad (20)$$

while  $\Delta_{Rrs}$  changes with  $a_{nw}$  through

$$\frac{\partial \Delta_{Rrs}}{\partial a_{nw}} = -2 \sum_{\lambda_1}^{\lambda_2} \left( A(\lambda) \frac{B_w(\lambda) + B_{nw}}{a_w(\lambda) + a_{nw}} - R_{rs}(\lambda) \right) A(\lambda) \frac{B_w(\lambda) + B_{nw}}{(a_w(\lambda) + a_{nw})^2} \quad (21)$$

For a given  $a_{nw}$ , there is a value of  $B_{nw}$  that makes  $\frac{\partial \Delta_{Rrs}}{\partial B_{nw}}$  equal to zero (same for  $a_{nw}$ ). When optimization is reached, both  $\frac{\partial \Delta_{Rrs}}{\partial B_{nw}}$  and  $\frac{\partial \Delta_{Rrs}}{\partial a_{nw}}$  reach zero. Furthermore,  $\frac{\partial \Delta_{Rrs}}{\partial B_{nw}}$  is negative (negative slope) when  $B_{nw}$  is smaller than the optimized  $B_{nw}$  value, and  $\Delta_{Rrs}$  decreases with the increase of  $B_{nw}$  toward the optimum value; similarly,  $\frac{\partial \Delta_{Rrs}}{\partial B_{nw}}$  is positive (positive slope) when  $B_{nw}$  is larger than the optimized  $B_{nw}$  value, and  $\Delta_{Rrs}$  increases with the increase of  $B_{nw}$  away from the optimum value. This monotonic behavior on either side of the global minimum just illustrates that there is no local minimum.

If  $a_{nw}$  (or  $B_{nw}$ ) is modeled with two or more components (e.g., Eq. 13), the variation of  $\Delta_{Rrs}$  for each individual component becomes more complex. In particular, it will depend on whether the two (or more) components are spectrally distinguishable enough, otherwise the solution for these components will not be unique and thus the separation cannot be resolved (such as the separation of absorption between detritus and gelbstoff). Fortunately, the spectral shapes between  $a_{ph}$  and  $a_{dg}$  are significantly different in the 410 – 670 nm range, which ensures a general resolution of these two components, although uncertainty of each derived component varies case by case [32] and the impact on both  $\frac{\partial \Delta_{Rrs}}{\partial a_{dg}}$  and  $\frac{\partial \Delta_{Rrs}}{\partial a_{ph}}$  is strong (see Figure 4).

#### 4.2 $\delta_{Rrs}^{min}$ distribution

The spectral models for IOPs not only affect the shape of the error function, but also the value of  $\delta_{Rrs}^{min}$  (a measure of closure). Figure 5a presents the  $\delta_{Rrs}^{min}$  values from both HOPE and GSM models for the 500 simulated data, respectively, and Figure 5b shows the distribution of the  $\delta_{Rrs}^{min}$  values. The X-axis of Figure 5a is roughly arranged in order from low-complexity, oligotrophic waters ( $a(440) \sim 0.016 \text{ m}^{-1}$ ) to higher-complexity, eutrophic waters ( $a(440) \sim 3.2 \text{ m}^{-1}$ ). Generally,  $\delta_{Rrs}^{min}$  from the HOPE model is smaller than that from the GSM model ( $\delta_{Rrs}^{min}$  is centered around 0.03 for HOPE while it spans between 0.04 and 0.10 for GSM). The  $\delta_{Rrs}^{min}$  value from the HOPE model increases with the complexity of the water, which is expected because, for eutrophic waters, it is less likely that the assumed  $\tilde{a}_{ph}(\lambda)$  matches perfectly the actual phytoplankton absorption spectrum. However, it is interesting and intriguing that the  $\delta_{Rrs}^{min}$  value of GSM increases then decreases with the increasing of complexity.

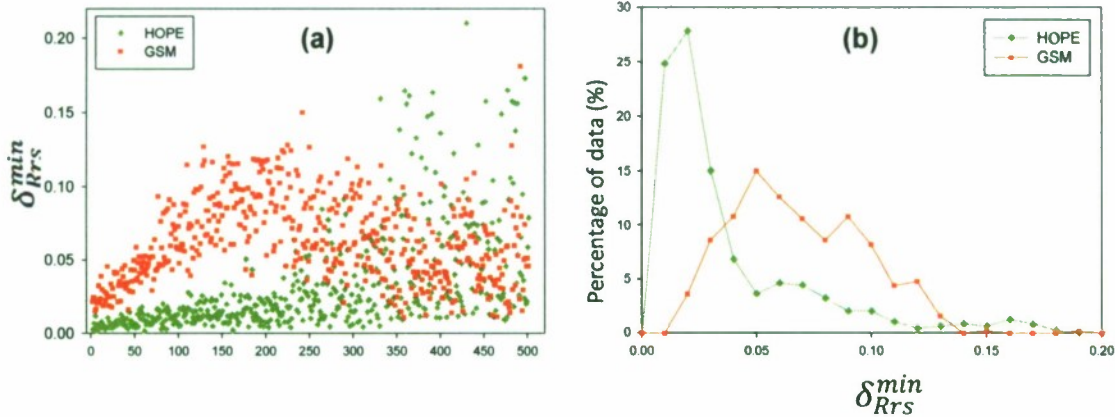


Figure 5. Values and distributions of  $\delta_{Rrs}^{min}$  from HOPE and GSM.

### 4.3 $\delta_{IOP}$ distribution

After optimization was achieved, the derived spectral models of the IOPs were compared with the known IOP inputs used to generate the simulated  $R_{rs}$  spectra to measure the quality of the SOA retrievals. Different from the usual evaluation of retrieved IOPs at a single wavelength, the scheme here basically considers the IOP spectrum as a whole. This is valuable because both the quantity and quality of the sub-surface light field are determined by the IOP spectra. Figures 6-9 present the values of  $\delta_{IOP}$  (spectra of total absorption, phytoplankton absorption, detritus-gelbstoff absorption, and particle backscattering, respectively) obtained from both HOPE and GSM.  $\delta_{IOP}$  is calculated following Eq. 2, but restricting the wavelength range to 410-555 nm, as the longer wavelength (670 nm here) has limited information of the active optical components. A few general points are observed for this dataset:

- $\delta_{IOP}$  of HOPE is smaller than that of GSM
- For absorption spectrum, mean  $\delta_a$  is  $\sim 8\%$  and smaller for low complexity (blue) waters (Figure 6) when HOPE is used
- $\delta_{aph}$  and  $\delta_{adg}$  are much higher than  $\delta_a$ , and  $\delta_{aph}$  of GSM is much higher than that of HOPE. This is probably because the  $\tilde{a}_{ph}(\lambda)$  used in GSM does not well represent the spectral shape observed from sample measurements
- $\delta_{Bp}$  of HOPE is centered  $\sim 10\%$  while  $\delta_{Bp}$  from GSM spans a range of  $\sim 10\text{-}50\%$ . Again,  $\delta_{Bp}$  from HOPE increases with increasing complexity, but  $\delta_{Bp}$  from GSM slightly decreases then increases with water complexity.

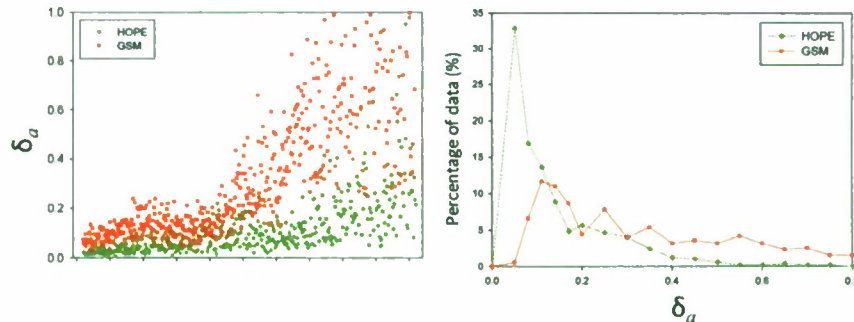


Figure 6. Values and distributions of  $\delta_a$ .

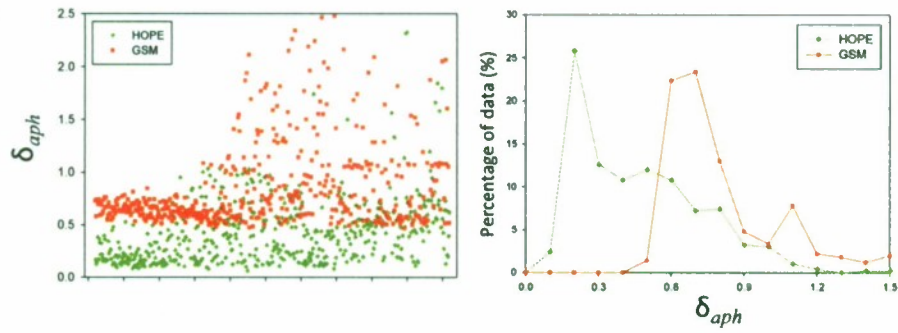


Figure 7. Values and distributions of  $\delta_{apl}$

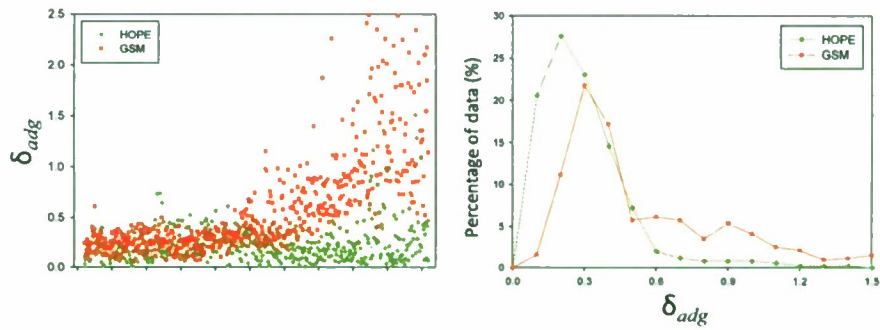


Figure 8. Values and distributions of  $\delta_{adg}$

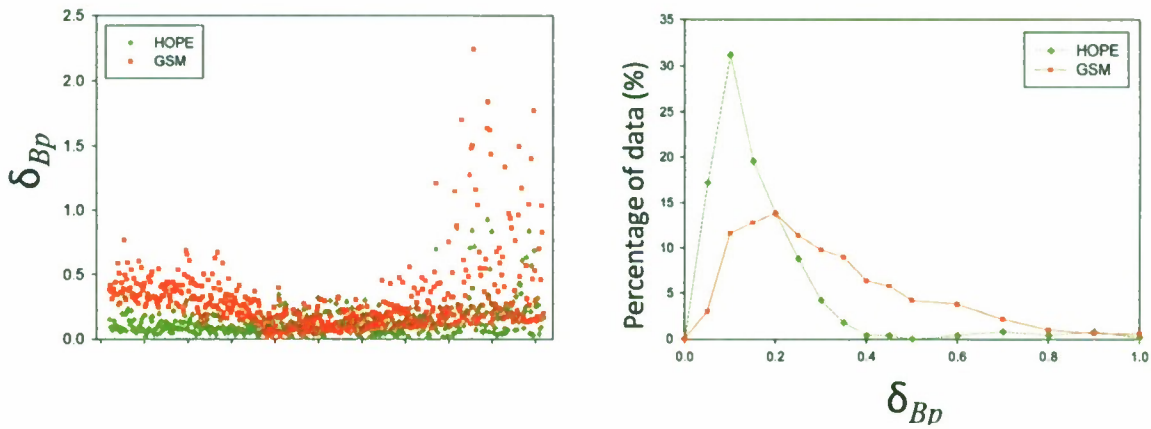


Figure 9. Values and distributions of  $\delta_{Bp}$

## 5. SUMMARY

With a simplified model for remote sensing reflectance, we proved that the error function used to measure the goodness-of-fit is in general a monotonic function of backscattering and absorption before and after the optimization point

(especially for blue waters with a spectral range of 400-700 nm). It is not possible for the SOA solution of such a model to become trapped in a local minimum before reaching the global minimum. However, this ultimately depends on other factors such as the complexity of the models and water properties and the spectral range and resolution of the observed spectral  $R_{rs}$ . Further, we applied two spectral model formulations (HOPE and GSM) to the IOCCG numerically simulated data and showed how the different model assumptions affect the closure between modeled and known  $R_{rs}$ , the surface shape of the error function, and the quality of SOA retrieved spectral IOPs. Results here further highlight the necessity and importance to develop and utilize appropriate models for the spectral shape of the IOPs for SOA schemes.

## ACKNOWLEDGEMENT

Financial support for this study was provided by NASA and NRL.

## REFERENCE

- [1] H. R. Gordon and A. Morel, "Remote assessment of ocean color for interpretation of satellite visible imagery: A review". New York: Springer-Verlag, 1983.
- [2] J. O'Reilly, *et al.*, "Ocean color chlorophyll algorithms for SeaWiFS," *J. Geophys. Res.*, vol. 103, pp. 24937-24953, 1998.
- [3] Z. P. Lee, *et al.*, "Deriving inherent optical properties from water color: A multi-band quasi-analytical algorithm for optically deep waters," *Applied Optics*, vol. 41, pp. 5755-5772, 2002.
- [4] T. J. Smyth, *et al.*, "Semianalytical model for the derivation of ocean color inherent optical properties: description, implementation, and performance assessment," *Appl. Opt.*, vol. 45, pp. 8116-8131, 2006.
- [5] Z. P. Lee, "Visible-infrared Remote-sensing Model and Applications for Ocean Waters," Ph. D, Department of Marine Science, The University of South Florida, St. Petersburg, 1994.
- [6] R. P. Bukata, *et al.*, *Optical Properties and Remote Sensing of Inland and Coastal Waters*. Boca Raton, FL: CRC Press, 1995.
- [7] C. S. Roesler and M. J. Perry, "In situ phytoplankton absorption, fluorescence emission, and particulate backscattering spectra determined from reflectance," *J. Geophys. Res.*, vol. 100, pp. 13279-13294, 1995.
- [8] R. Doerffer and J. Fisher, "Concentrations of chlorophyll, suspended matter, and gelbstoff in case II waters derived from satellite coastal zone color scanner data with inverse modeling methods," *J. Geophys. Res.*, vol. 99, pp. 7475-7466, 1994.
- [9] C. Hu, *et al.*, "Application of an optimization algorithm to satellite ocean color imagery: A case study in Southwest Florida coastal waters," in *Ocean Remote Sensing and Applications*, Hangzhou, China, 2002, pp. 70-79.
- [10] P. J. Werdell, "Global bio-optical algorithms for ocean color satellite applications," *AGU EOS Transactions* vol. 90, p. doi:10.1029/2009EO010005, 2009.
- [11] S. Maritorena and D. A. Siegel, "Consistent merging of satellite ocean color data sets using a bio-optical model," *Remote Sens. Environ.*, vol. 94, pp. 429-440, 2005.
- [12] V. E. Brando and A. G. Dekker, "Satellite hyperspectral remote sensing for estimating estuarine and coastal water quality," *IEEE Transactions on Geoscience and Remote Sensing*, vol. 41, pp. 1378-1387, 2003.
- [13] E. Devred, *et al.*, "A two-component model of phytoplankton absorption in the open ocean: Theory and applications," *J. Geophys. Res.*, vol. 111, pp. C03011, doi:10.1029/2005JC002880, 2006.
- [14] Z. P. Lee, *et al.*, "Hyperspectral remote sensing for shallow waters: 2. Deriving bottom depths and water properties by optimization," *Applied Optics*, vol. 38, pp. 3831-3843, 1999.
- [15] S. Maritorena, *et al.*, "Optimization of a semianalytical ocean color model for global-scale applications," *Applied Optics*, vol. 41, pp. 2705-2714, 2002.
- [16] S. Kirkpatrick, *et al.*, "Optimization by simulated annealing," *Science*, vol. 220, pp. 671-680, 1983.
- [17] M. Chami and D. Robilliard, "Inversion of Oceanic Constituents in Case I and II Waters with Genetic Programming Algorithms," *Applied Optics*, vol. 41, pp. 6260-6275, 2002.
- [18] C.-C. Liu, *et al.*, "Integrating semianalytical end genetic algorithms to retrieve the constituents of water bodies from remote sensing of ocean color," *Optical Express*, vol. 15, pp. 252-265, 2007.
- [19] H. R. Gordon, *et al.*, "A semianalytic radiance model of ocean color," *J. Geophys. Res.*, vol. 93, pp. 10,909-10,924, 1988.

- [20] A. Morel and B. Gentili, "Diffuse reflectance of oceanic waters (2): Bi-directional aspects," *Applied Optics*, vol. 32, pp. 6864-6879, 1993.
- [21] IOCCG, "Remote Sensing of Inherent Optical Properties: Fundamentals, Tests of Algorithms, and Applications," in *Reports of the International Ocean-Colour Coordinating Group, No. 5*. vol. 5, Z.-P. Lee, Ed., ed Dartmouth, Canada: IOCCG, 2006, p. 126.
- [22] Z.-P. Lee, *et al.*, "An inherent-optical-property-centered approach to correct the angular effects in water-leaving radiance," *Applied Optics*, vol. 50, pp. 3155-3167, 2011.
- [23] S. Sathyendranath, *et al.*, "A three-component model of ocean colour and its application to remote sensing of phytoplankton pigments in coastal waters," *Int. J. Remote Sensing*, vol. 10, pp. 1373-1394, 1989.
- [24] W. S. Pegau, *et al.*, "Absorption and attenuation of visible and near-infrared light in water: dependence on temperature and salinity," *Applied Optics*, vol. 36, pp. 6035-6046, 1997.
- [25] Z. P. Lee, *et al.*, "Hyperspectral remote sensing for shallow waters. 1. A semianalytical model," *Applied Optics*, vol. 37, pp. 6329-6338, 1998.
- [26] A. Bricaud, *et al.*, "Variability in the chlorophyll-specific absorption coefficients of natural phytoplankton: Analysis and parameterization," *J. Geophys. Res.*, vol. 100, pp. 13321-13332, 1995.
- [27] A. Bricaud, *et al.*, "Absorption by dissolved organic matter of the sea (yellow substance) in the UV and visible domains," *Limnol. Oceanogr.*, vol. 26, pp. 43-53, 1981.
- [28] A. Bricaud and D. Stramski, "Spectral absorption coefficients of living phytoplankton and nonalgal biogenous matter: A comparison between the Peru upwelling area and the Sargasso Sea," *Limnol. Oceanogr.*, vol. 35, pp. 562-582, 1990.
- [29] A. M. Ciotti, *et al.*, "Assessment of the relationships between dominant cell size in natural phytoplankton communities and spectral shape of the absorption coefficient," *Limnol. Oceanogr.*, vol. 47, pp. 404-417, 2002.
- [30] L. S. Lasdon, *et al.*, "Design and testing of generalized reduced gradient code for nonlinear programming," Stanford CA, 1976.
- [31] D. Fylstra, *et al.*, "Design and Use of the Microsoft Excel Solver," *Interfaces*, vol. 28, pp. 29-55, 1998.
- [32] Z.-P. Lee, *et al.*, "Uncertainties of optical parameters and their propagations in an analytical ocean color inversion algorithm," *Applied Optics*, vol. 49, pp. 369-381, 2010.